Multifunctional Oval-Shaped Gold-Nanoparticle-Based Selective Detection of Breast Cancer Cells Using Simple Colorimetric and Highly Sensitive Two-Photon Scattering Assay

Wentong Lu, Sri Ranjini Arumugam, Dulal Senapati, Anant K. Singh, Tahir Arbneshi, Sadia Afrin Khan, Hongtao Yu, and Paresh Chandra Ray*

Department of Chemistry, Jackson State University, Jackson, Mississippi 39217

ABSTRACT Breast cancer is the most common cancer among women, and it is the second leading cause of cancer deaths in women today. The key to the effective and ultimately successful treatment of diseases such as cancer is early and accurate diagnosis. Driven by the need, in this article, we report for the first time a simple colorimetric and highly sensitive two-photon scattering assay for highly selective and sensitive detection of breast cancer SK-BR-3 cell lines at a 100 cells/mL level using a multifunctional (monoclonal anti-HER2/c-erb-2 antibody and S6 RNA aptamer-conjugated) oval-shaped gold-nanoparticle-based nanoconjugate. When multifunctional oval-shaped gold nanoparticles are mixed with the breast cancer SK-BR-3 cell line, a distinct color change occurs and two-photon scattering intensity increases by about 13 times. Experimental data with the HaCaT noncancerous cell line, as well as with MDA-MB-231 breast cancer cell line, clearly demonstrated that our assay was highly sensitive to SK-BR-3 and it was able to distinguish from other breast cancer cell lines that express low levels of HER2. The mechanism of selectivity and the assay's response change have been discussed. Our experimental results reported here open up a new possibility of rapid, easy, and reliable diagnosis of cancer cell lines by monitoring the colorimetric change and measuring TPS intensity from multifunctional gold nanosystems.

KEYWORDS: breast cancer · oval-shaped gold nanoparticle · two-photon scattering · plasmonics · colorimetric

Cancer has been described in early medical texts from antiquity, but until now, it remains the second leading cause of death in our world.[1−5] Breast cancer is the most common cancer among women, and it is the second leading cause of cancer deaths in women today, after lung cancer.[3−5] Rapid selective detection of cancer cells is an important challenge for the diagnosis and treatment of tumors.[1−9] The key to the effective and ultimately successful treatment of diseases such as cancer is an early and accurate diagnosis. With oncogenes, such as human epidermal growth factor receptor 2 (HER2)/Neu, overexpression is found in about 30% of different breast cancer cases and 20% of ovarian cancer cases.[1−24] Also, there is mounting evidence for the role of HER2 overexpression in patients with gastric cancer.[1−18] As a result, immunophenotypic analysis of cancer cells using antibody probes for specific surface antigens has limitations due to the fact that antigens used for cell recognition are normally not exclusively expressed on any single cell type, dramatically influencing selectivity and resulting in false positive signals.[13,16,17] Target cell-specific aptamers have the potential to serve as molecular probes for specific recognition of the cancerous cells from complex mixtures including whole blood samples.[5,13,14,16,17] Most aptamers reported for breast cancer cell lines have weak binding affinity and thus low signal in molecular imaging, limiting their ability for highly sensitive detection of cancer cells.[5,16,17] In addition, during the early stages of cancer development, cancer cells will have a very low density of target membrane proteins for recognition of a specific cancer cell. In this case, single aptamer/antibody binding will not be enough to detect early stage cancer development.[1−17] Given the complexity and diversity of cancers, in order to increase sensitivity and selectivity, multivalent binding is usually considered to be essential for early stage disease diagnostics.[1−30] To address this, in this article, we report the use of an oval-shaped gold-nanoparticle-based multifunctional (antibody and aptamer) nanoconjugate platform for highly selective and sensitive detection of a breast cancer cell line (as shown in Scheme 1). Since the nanoparticle provides a large surface area, it will be easier to incorporate several

*Address correspondence to paresh.c.ray@jsums.edu.

Received for review December 1, 2009 and accepted February 03, 2010.

Published online February 15, 2010.
10.1021/nn901742q

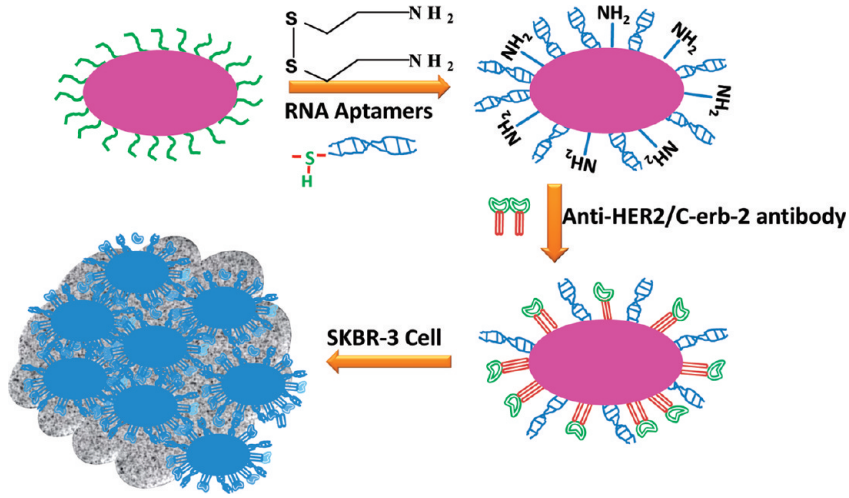

Scheme 1. First two steps show schematic representation of the synthesis of monoclonal anti-HER2 antibody and S6 RNA aptamer-conjugated oval-shaped gold nanoparticles. Third step shows schematic representation of multifunctional oval-shaped gold-nanoparticle-based sensing of the SK-BR-3 breast cancer cell line.

recognition elements in the same surface. A well-characterized breast cancer cell line, SK-BR-3, which overexpresses the epithermal growth factor receptor HER2/c-erb-2/Neu (HER2) on the cell surface, has been used to demonstrate the ultrasensitive detection capability. For selective and sensitive detection of the SK-BR-3 cell line, we have conjugated oval-shaped gold nanoparticles by multiple HER2 specific targets, and these are anti-HER2 antibody and S6 RNA aptamer (kd = 94.6 nM[5]). Both of them are known to exhibit highly specific targeting for the SK-BR-3 cell line.[4−7]

Due to the unique optical properties of nanomaterials, over the last 5 years, several groups have been developing suitable nanomaterials for cancer imaging and therapy.[5−20] In noble metal gold nanoparticles, the coherent collective oscillation of electrons in the conduction band induces large surface electric fields, which greatly enhances the radiative properties of these nanoparticles.[5−42] As a result, the light scattering cross section of metal nanoparticles is several orders of magnitude more intense than that of organic dyes, which makes it an excellent candidate for sensor development and novel contrast agents for optical detection.[15−57] In the last couple of years, several publications[27,28,50−57] have shown that two-photon scattering (TPS) properties can be greatly enhanced ($\sim 10^4-10^6$) for molecules on a roughened *versus* an unroughened metal surface, which is comparable to very large enhancements (10^4-10^{14}) observed in surface-enhanced Raman scattering (SERS) from organic dyes on colloidal solution.[29−41] Average SERS enhancement on the order of 10^4-10^8 have been reported,[35−39,41] and in case of single molecule SERS experiments, enhancements as high as 10^{14} have been reported.[29−32,40] Using the above unique two-photon optical property of gold nanoparticles, we report here that the TPS properties of oval-shaped gold nanoparticles can be used for rapid, highly sensitive and selective detection of the SK-BR-3 human breast cancer cell line. The TPS or hyper-Rayleigh scattering technique[27,28,50−62] is based on light scattering. TPS can be observed from fluctuations in symmetry, caused by rotational fluctuations, where scattering by a fundamental laser beam can be detected at the second harmonic wavelength.[50−62] Our group and other groups have demonstrated that this technique can easily be applied to study a very wide range of materials because electrostatic fields and phase matching are not required.[27,28,50−62]

RESULTS AND DISCUSSION

Our oval-shaped gold-nanoparticle-based colorimetric and two-photon scattering approach for the detection of selective SK-BR-3 cell line is based on the fact that multifunctional conjugated oval-shaped gold nanoparticles can readily and specifically identify the breast cancer cell line through HER2/c-erb-2/Neu receptor recognition (as shown in Scheme 1). For the SK-BR-3 cell line, there are many surface epithermal growth factor receptors (HER2/c-erb-2/Neu) available for specific recognition with monoclonal anti-HER2/c-erb-2 antibody and S6 aptamer-conjugated oval-shaped gold nanoparticle. Therefore, in the presence of the SK-BR-3 cell line, several nanoparticles can bind to HER2 receptors in the cancer cell, thereby producing nanoparticle aggregates (as shown in Scheme 1). Our TEM image (as shown in Figure 1B) shows clearly that a multifunctional nanoparticle and SK-BR-3 cancer cell interaction is highly specific, and nanoparticles are strong aggregates on the surface of cancer cells. As a result, a colorimetric change has been observed from pink to bluish color (as shown in Figure 2B), and a new broad band appears around 150 nm far from their plasmon absorption band, as shown in Figure 2A. This red shift might be due to two factors. One is the change in the local refractive index on the nanoparticle surface caused by the specific binding of the multifunctional nanoparti-

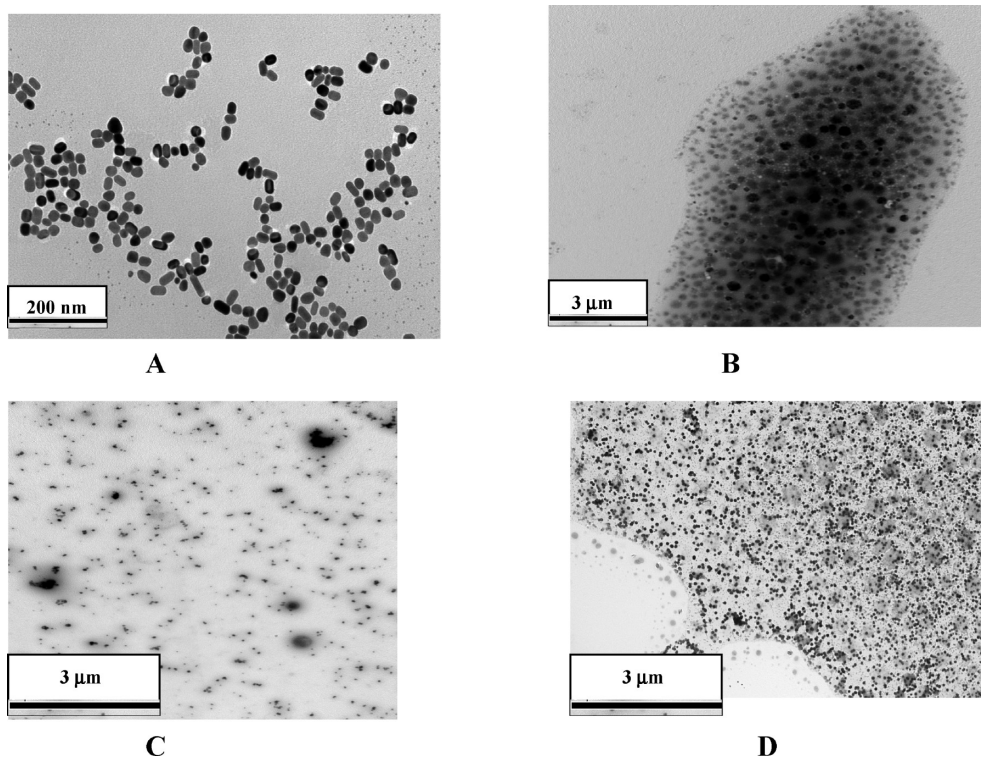

Figure 1. (A) TEM image showing anti-HER2 antibody and S6 RNA aptamer-conjugated oval-shaped gold nanoparticles before addition of the cell line. (B) TEM image demonstrating aggregation of multifunctional oval-shaped gold nanoparticles after the addition of 10^4 SK-BR-3 cells/mL. (C) TEM image showing very little aggregation after the addition of 10^4 MDA-MB-231 cells/mL on multifunctional oval-shaped gold nanoparticles. (D) TEM image demonstrating almost no aggregation after the addition of 10^4 HaCaT cells/mL, where nanoparticles are randomly distributed on the whole cells.

cle (NP), which binds to HER2/c-erb-2 on the SK-BR-3 cell surface. The other is the interparticle interaction resulting from the assembly of nanoparticles on the cell surface.[6−50] As shown in Figure 2B, the colorimetric pattern of oval-shaped gold nanoparticles remains unchanged when we added an anti-HER2 antibody/S6 RNA aptamer-coated NP to the HaCaT noncancerous cells as well as MDA-MB-231 breast cancer cell line. As shown in Figure 1D, our TEM image also clearly demonstrated that the HaCaT noncancerous cells are poorly labeled by the nanoparticles, and as a result, we have not observed clear colorimetric change. As noted from Figure 1D, some oval-shaped gold nanoparticles are also found on the HaCaT noncancerous cells, and it is mostly due to the nonspecific interactions between the antibodies and the proteins on the cell surface, and thus the nanoparticles are randomly distributed on the whole cells. As a result, we have not observed the colorimetric change as we observed for the SK-BR-3 cell line.

Figure 1C shows a TEM image that clearly demonstrates that the MDA-MB-231 breast cancerous cells are also quite poorly labeled by the nanoparticles, and as a result, we have not observed clear colorimetric change. MDA-MB-231 is the breast cancer cell line that expresses low levels of HER2, and as a result, there is a weak interaction between the monoclonal anti-HER2/c-erb-2 antibody and S6 aptamer-conjugated oval-shaped gold nanoparticle and the MDA-MB-231 cancer cell line. Due to the lack of strong interaction, nanoparticles do not produce larger aggregates, and as a result, no color change has been observed. This contrast difference clearly demonstrates that our multifunctional oval-shaped gold-nanoparticle-based colorimetric assay is highly specific for SK-BR-3 cancer cell lines and it can even distinguish between different breast cancer cell lines. To evaluate the sensitivity of our multifunctional oval-shaped gold-nanoparticle-based colorimetric assay, different concentrations of SK-BR-3 cells from one stock solution were evaluated. As shown in Figure 2C, our colorimetric assay is highly sensitive to the concentration of SK-BR-3 cancer cells. Our result clearly shows that the sensitivity of the colorimetric assay is 10^4 cells/mL.

To improve the assay sensitivity toward SK-BR-3 cancer cell detection, we have employed a TPS technique.[27,28,50−62] TPS is a powerful method to determine the small change in the size of the particles, and therefore, even it has the capability to separate dimer from the monomer.[27,28,50−57] As shown in Figure 3A, when monoclonal anti-HER2/c-erb-2 antibody and S6 aptamer-conjugated oval-shaped gold nanoparticles were mixed with various concentrations of SK-BR-3 cells, two-photon scattering intensity increases by about 13 times (as shown in Figure 3A). Our experimental results demonstrated a very distinct two-photon

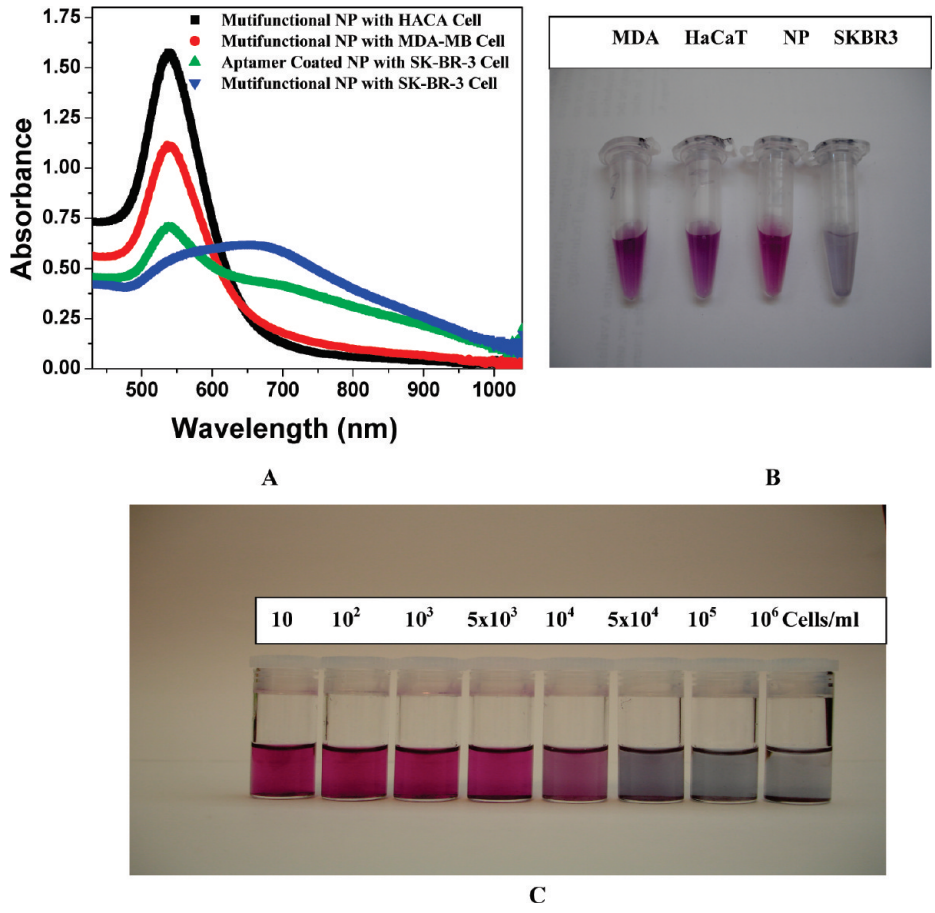

Figure 2. (A) Absorption profile variation of multifunctional oval-shaped gold nanoparticles due to the addition of different cancerous and noncancerous cells. (B) Photograph showing colorimetric change upon addition of different cancer cells (10^4 cells/mL). (C) Photograph demonstrating colorimetric change upon the addition of different numbers of SK-BR-3 cells.

scattering intensity change even upon the addition of 100 SK-BR-3 cancer cells/mL, whereas we observed colorimetric change only after addition of 10^4 cells/mL (shown in Figure 2C). So our result clearly shows that TPS assay is 2 orders of magnitude more sensitive than the normal colorimetric assay.

Two-photon scattering signal from multifunctional gold nanoparticles can be expressed as[27,28,50−63]

$$I_{TPRS} = G\langle N_w\beta_w{}^2 + N_{nano}\beta_{nano}{}^2\rangle I_\omega{}^2 e^{-N_{nano}\varepsilon_{2\omega}} \quad (1)$$

where G is a geometric factor, N_w and N_{nano} are the number of water molecules and monoclonal anti-tau antibody-conjugated gold nanoparticle per unit volume, β_w and β_{nano} are the quadratic hyperpolarizabilities of a single water molecule and a single monoclonal anti-tau antibody-conjugated gold nanoparticle, $\varepsilon_{2\omega}$ is the molar extinction coefficient of the gold nanoparticle at 2ω, l is the path length, and I_ω the fundamental intensity. The exponential factor accounts for the losses through absorption at the harmonic frequency. Considering the size of the nanoparticle, the approximation that assumes that the electromagnetic fields are spatially constant over the volume of the particle may not be suitable anymore. As a result, the total nonlinear polarization consists of different contributions such as multipolar radiation of the harmonic energy of the excited dipole and possibly of higher multipoles, as we discussed in our previous publication or reported by others.[27,28,50−57]

The TPS intensity change upon aggregation of multifunctional oval-shaped gold nanoparticles in the presence of the SK-BR-3 cell line consists of several contributions: (1) The first one is the electric dipole approximation, which may arise due to the defects in the nanoparticle. This contribution is actually identical to the one observed for any noncentrosymmetrical point-like objects.[57−63] After the aggregation in the presence of SK-BR-3 cells, multifunctional oval-shaped gold nanoparticles lose the center of symmetry, and as a result, one can expect a significant amount of electric dipole contribution to the two-photon scattering intensity. Since the electric dipole contributes several times higher than that of multipolar moments, we expect two-photon scattering intensity to increase upon the addition of SK-BR-3 cells. (2) The second contribution is multipolar contribution like electric quadrupole contribution.[27,28,50−57] This contribution is very important when aggregation occurs due to the addition of SK-BR-3 cells. Since after aggregation the size of the particle is no longer negligible compared to the wave-

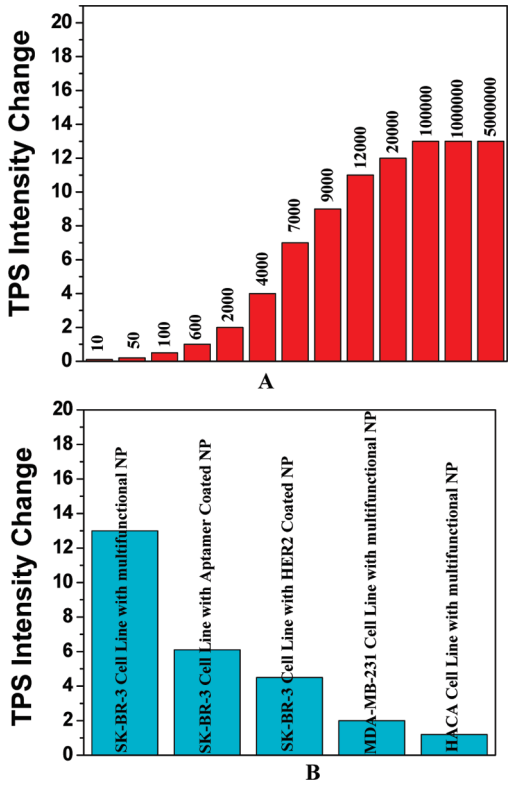

Figure 3. (A) Plot demonstrating two-photon scattering intensity changes upon the addition of different concentrations (number of cells/mL) of SK-BR-3 breast cancerous cells on multifunctional oval-shaped gold nanoparticles. (B) Plot demonstrating selectivity of our TPS assay over other cancerous and noncancerous cell lines. Two-photon scattering intensity changes only two times upon the addition of 10^5 MDA-MB-231 breast cancerous cells, whereas TPS intensity changes 13 times upon the addition of the same number of SK-BR-3 cells.

length, one cannot neglect multipolar contribution, as we and others reported before.[27,28,50−57] As a result, after aggregation, one can expect very high multipolar contribution. To probe the multipolar contribution, we performed angle-resolved HRS measurement. For this purpose, the fundamental input beam was linearly polarized, and the input angle of polarization was selected with a rotating half-wave plate. The configuration of the experimental setup was such that the fundamental beam was propagating in the *Z* direction with the electric field polarized in the {*X*,*Y*} plane with the polarization angle, and the harmonic light was collected along the *Y* direction, at a right angle from the fundamental beam propagation direction.

As shown in Figure 4A, our experimental plot shows two lobes for multifunctional oval-shaped gold nanoparticles, which are similar to the one for pure electric dipole response from noncentrosymmetric organic molecules, as reported before by several groups.[60−63] As shown in Figure 4B, in the presence of the cancer cell line, the nature of the plot changes significantly. A polar plot contribution pattern shows clearly four lobes. The asymmetric four-lobe pattern is no longer predominantly dipolar in origin. Therefore, our experimental observation shows that, due to the aggregation in the presence of the cancer cell, one cannot neglect multipolar contribution, and the origin of the very high nonlinearity after the addition of SK-BR-3 cells is due to the presence of both dipolar and multipoar contributions. (3) The third contribution is the resonance contribution. As shown in Figure 1D, a clear colorimetric change is observed when SK-BR-3 cells were added to multifunctional oval-shaped gold nanoparticles, and as a result, absorption spectra shifted 150 nm, as shown in Figure 1E. Now this new absorption band appearing at 700 nm upon the addition of the SK-BR-3 cell line can influence the TPRS intensity very highly due to single photon resonance. According to the two-state model[63]

$$\beta^{\text{two-state}} = \underbrace{\frac{3\mu_{eg}^{\,2}\Delta\mu_{eg}}{E_{eg}^{2}}}_{\text{static factor}} \underbrace{\frac{\omega_{eg}^{\,4}}{(\omega_{eg}^{\,2} - 4\omega^2)(\omega_{eg}^{\,2} - \omega^2)}}_{\text{dispersion factor}} \quad (2)$$

where ω is the fundamental energy of the incident light, μ_{eg} is the transition dipole moment, and ω_{eg} is the transition energy between the ground state $|g\rangle$ and the charge-excited state $|e\rangle$, $\Delta\mu_{eg}$ is the difference in dipole moment between $|e\rangle$ and $|g\rangle$ states. Since

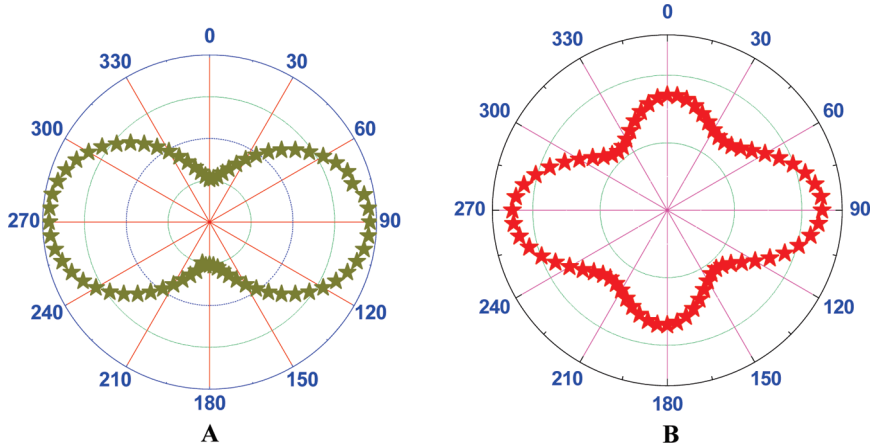

Figure 4. Polar plot of the HRS intensity as a function of the incoming fundamental beam polarization angle (φ) from multifunctional oval-shaped gold nanoparticle (A) before addition of cancer cells and (B) after the addition of cancer cells.

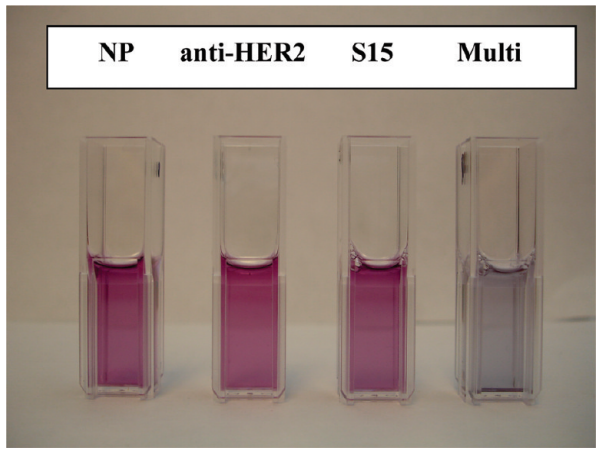

Figure 5. Photograph showing colorimetric change only when multifunctional oval-shaped gold nanoparticles have been used.

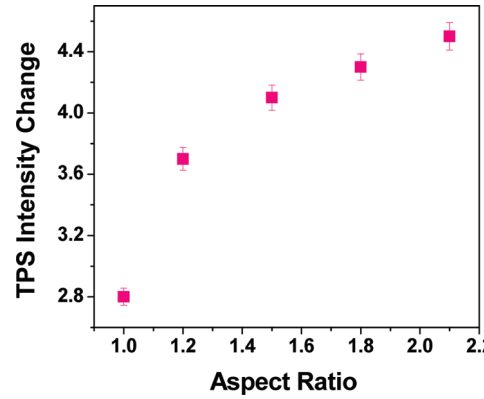

Figure 6. Aspect ratio dependent TPS intensity change upon the addition of SK-BR-3 cancer cells to multifunctional gold nanoparticles.

$\omega_{eg} \propto 1/\lambda_{max}$, β should change tremendously upon the addition of SK-BR-3 cells, and as a result, the two-photon scattering intensity should change tremendously with the addition of SK-BR-3 cells. (4) The fourth contribution is due to the size-dependent scattering properties. Since size increases tremendously with aggregation, the two-photon scattering intensity should increase with the increase in particle size.

To evaluate whether our assay is highly selective, we have also shown how two-photon scattering intensity changes upon addition of HaCaT noncancerous cells and the MDA-MB-231 breast cancer cell line. As shown in Figure 3B, two-photon scattering intensity changes only 1.3 times in the presence of 10^5 HaCaT cells/mL and 2.2 times when we added 10^5 MDA-MB-231 breast cancer cells/mL to multifunctional oval-shaped gold nanoparticles. So our experiments clearly demonstrate that our multifunctional oval-shaped gold-nanoparticle-based two-photon scattering assay is highly specific for SK-BR-3 cancer cell lines and it can even distinguish between different breast cancer cell lines.

To understand the colorimetric and TPS assay responses with a single biofunctional nanoparticle, we have also performed experiments on the addition of 10^5 SK-BR-3 cancer cells/mL, with only S6 RNA aptamer-conjugated oval-shaped gold nanoparticles or anti-HER2/c-erb-2 antibody-conjugated nanoparticles, as well as multifunctional nanoparticles. Figure 5 clearly demonstrates that colorimetric change was only observed when we used multifunctional gold nanoparticles. No colorimetric change was observed for a single biofunctional nanoparticle. As shown in Figure 3B, TPS intensity changes only 4.1 times when SK-BR-3 cancer cells were added to anti-HER2/c-erb-2 antibody-conjugated nanoparticles and around 6.1 times in the case of S6 RNA aptamer-conjugated oval-shaped gold nanoparticle, whereas TPS intensity changes 13 times when we used multifunctional nanoparticles. So by using multifunctional gold nanoparticles, we increased our TPS assay signal more than twice as much.

To understand whether our TPS assay sensitivity varies with the aspect ratio (length/diameter) of gold nanoparticle, we have performed our experiment using 1−2.4 aspect ratio (σ) of different gold nanoparticles, where $\sigma = 1$ denotes spherical gold nanoparticles. Our experimental results (as shown in Figure 6) show that TPS intensity change is highly dependent on the aspect ratio of gold nanoparticles. As the particle aspect ratio increases, TPS intensity change becomes higher and higher, which indicates that sensitivity becomes better. This variation of sensitivity efficiency with particle aspect ratio can be due to the increase in surface area as well as higher contribution from multipolar moments.

In the past 15 years, surface-enhanced Raman scattering technique has been shown to be unique for ultrasensitive biological and chemical analysis and cancer cell imaging.[29−41] To compare the sensitivity of our TPS technique with established SERS technique,[29−41] we have also performed Raman-tagged Rhodamine 6G (Rh-6G)-labeled multifunctional gold-nanoparticle-based SERS for SK-BR-3 cell detection. We have used a continuous wavelength DPSS laser from laser glow technology (LUD-670) operating at 670 nm as an excitation light source and miniaturized QE65000 scientific-grade spectrometer from Ocean Optics as a Raman detector.[41] The spectral response range of this mini-Raman spectrometer is 220−3600 cm^{-1}. Detailed experimental setup has been reported recently by our group.[41] The Raman spectrum was collected with Ocean Optics data acquisition SpectraSuite spectroscopy software. As we discussed before, since in the presence of the SK-BR-3 cell line multifunctional gold nanoparticles undergo aggregation, it formed several hot spots and provided a significant enhancement of the Raman signal intensity by several orders of magnitude through electromagnetic field enhancements (as shown in Figure 7). The Raman modes at 236, 252, 273, and 376 cm^{-1} are N−C−C bending modes of the ethylamine group of the Rh-6G

ring, and the Raman modes at 615, 778, 1181, 1349 1366, 1511, 1570, 1603, and 1650 cm^{-1} are due to C−C−C ring in-plane bending, C−H out-of-plane bending, C−N stretching, and C−C stretching, as we reported before.[41,64]

To evaluate the sensitivity of the SERS probe, different concentrations of SK-BR-3 from one stock solution were evaluated. As shown in Figure 7, the SERS intensity is highly sensitive to the concentration of SK-BR-3. Our experimental results show that the detection capability of the SERS probe is as low as 40 SK-BR-3 cells, which is 2.5 times more sensitive than our TPS probe. Though our experimental results shows that SERS is a highly promising technology to detect SK-BR-3 cells at very low concentration, the necessity of Raman dye tagging makes it difficult to use it as a biosensor for real life application.

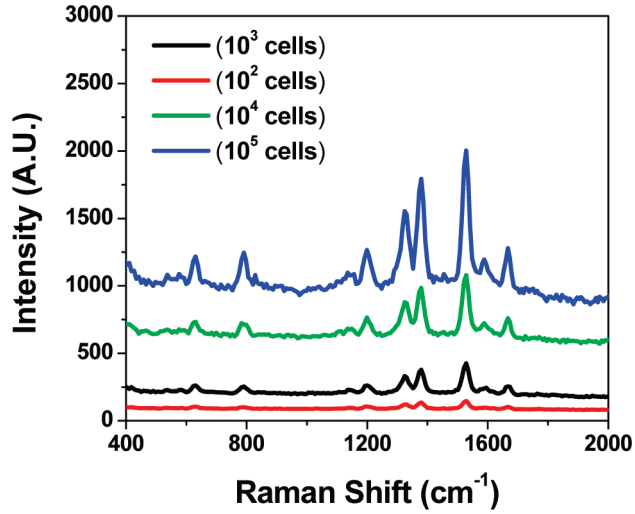

Figure 7. SERS spectra from Rh-6G-modified multifunctional gold nanoparticle in the presence of the different concentrations of SK-BR-3 cells (cells/mL).

CONCLUSION

In conclusion, in this article, we have demonstrated a label-free, fast, and highly sensitive multifunctional (monoclonal anti-HER2/c-erb-2 antibody and S6 RNA aptamer-conjugated) oval-shaped gold-nanoparticle-based simple colorimetric and highly sensitive two-photon scattering assay for the selective detection of breast cancer SK-BR-3 cell line at the 100 cells/mL level. We have shown that when multifunctional oval-shaped gold nanoparticles were mixed with breast cancer SK-BR-3 cell line, a distinct color change occurs and two-photon scattering intensity increases by about 13 times. Our experimental data with the HaCaT noncancerous cell line, as well as with MDA-MB-231 breast cancer cell line, clearly demonstrated that our colorimetric and TPS assay is highly sensitive to SK-BR-3 and it can distinguish it from other breast cancer cell lines that express low levels of HER2. Our experiment indicates that this bioassay is quite rapid, and it can be 2 orders of magnitude more sensitive than the usual colorimetric technique. We have also shown that, by using multifunctional gold nanoparticles, we are able to see colorimetric change directly upon the addition of the cancer cell line; also, using multifunctional nanoparticles, the TPS assay signal increases more than twice as much. Although we have shown promising advances in multifunctional oval-shaped gold-nanoparticle-based colorimetric and TPS assay, we still need a much greater understanding of how to control surface architecture in order to stabilize and maximize the assay response. Continued optimization of different parameters is necessary to monitor cancer cell lines in point of care complex environments. We believe that the assay has enormous potential for application of cancer cell detection from clinical samples.

MATERIALS AND EXPERIMENTS

Hydrogen tetrachloroaurate ($HAuCl_4 \cdot 3H_2O$), $NaBH_4$, sodium citrate, CTAB, and silver nitrate were purchased from Sigma-Aldrich and used without further purification. Monoclonal anti-HER2/c-erb-2 antibodies were purchased from Thermo Fisher Scientific, 3′-SH-modified S6 RNA aptamers were purchased from Midland Certified Reagent. The human adenocarcinoma breast cell line SK-BR-3, which overexpresses HER2/c-erb-2 gene product, was obtained from the American Type Culture Collection (ATCC, Rockville, MD). MDA-MB-231 breast cancer cell line was also purchased from ATCC. Human skin HaCaT keratinocytes, a transformed human epidermal cell line, was obtained from Dr. Norbert Fusenig of the Germany Cancer Research Center, Heidelberg, Germany.

Synthesis of Oval-Shaped Gold Nanoparticles. Oval-shaped gold nanoparticles (aspect ratio 1.3, as shown in Figure 7A) were synthesized using a seed-mediated growth procedure in the presence of CTAB. At first, we made a gold nanoseed (~3 nm diameter particles) using $NaBH_4$ reduction method as reported before. To prepare oval-shaped gold nanoparticles, we used 4.75 mL of 0.0085 M CTAB solution in a small vial, and then we added 0.2 mL of 0.01 M $HAuCl_4 \cdot 3H_2O$ under constant stirring. After that, we used 0.03 mL of 0.01 M $AgNO_3$ dropwise to allow the solution to mix properly. Once the solution was mixed properly, we added 0.032 mL of 0.1 M ascorbic acid slowly, as a reducing agent. The solution turned colorless. To this colorless solution, we added 0.01 mL of gold-seed at a time and gently mixed the solution for 30 s. Color changed immediately and became dark blue within 2 min. TEM image shows (Figure 8) that the aspect ratio of these oval-shaped nanoparticle is 1.3. This oval-shaped gold nanoparticle has only one plasmon-bond-like spherical gold nanoparticle, but their λ_{max} values shifted about 35 nm, in comparison to the spherical gold nanoparticle of the same size.

Preparation of Multifunctional Oval-Shaped Nanoconjugates. Oval-shaped gold nanoparticles (aspect ratio 1.3, as shown in Figure 8A) were synthesized using a seed-mediated growth procedure in the presence of CTAB. The above procedure produced oval-shaped gold nanoparticles with CTAB coating. CTAB is known to be cytotoxic, and as a result, it will not be ideal for *in vivo* diagnosis. Furthermore, CTAB is positively charged at physiological pH and will be able to attract negatively charged proteins easily. As a result, CTAB-coated oval-shaped gold nanoparticles can face severe nonspecific binding problems. To overcome this problem, we have modified the oval-shaped gold nanoparticle surface by -3′-SH-S6 RNA aptamers and cystamine dihydrochloride (as shown in Scheme 1) using a reported method.[55,56] The

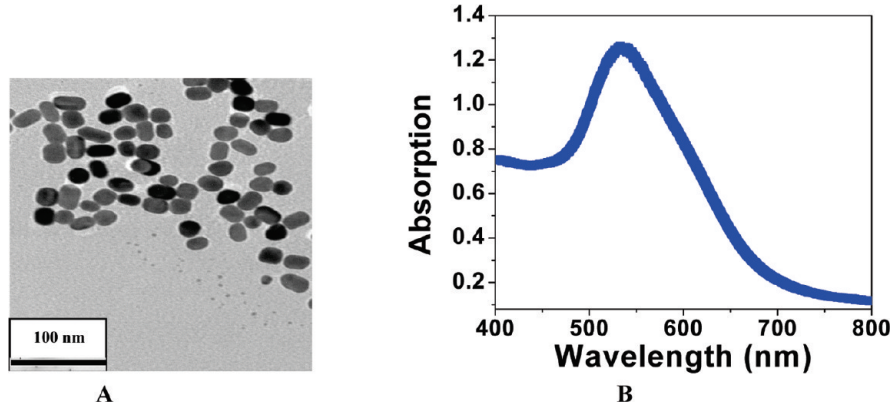

Figure 8. (A) TEM image showing oval-shaped gold nanoparticles (14 nm length and 18 nm width). (B) Absorption profile of oval-shaped gold nanoparticles.

−SH-labeled RNA aptamers were gradually exposed to gold nanomaterial in the presence of 0.1 M NaCl in a PBS buffer over a 16 h period according to a procedure we reported previously.[55,56] To remove the unbound RNA, we centrifuged the solution at 13 000 rpm for 20 min, and the precipitate was redispersed in 2 mL of the buffer solution. We continued this process three times. To measure the number of aptamer molecules in each gold nanoparticle, we performed the above process with Cy3-labeled RNA aptamers. After conjugation, we have treated the aptamer-conjugated gold nanoparticle with 10 μM potassium cyanide to oxidize the gold nanoparticle. After that, the solutions containing the released Cy3-labeled aptamers were collected for the fluorescence analyses. The amount of Cy3-labeled aptamers was measured by fluorescence. By dividing the total number of Cy3-labeled aptamers by the total number of nanoparticles, we estimated that there were about 600−700 aptamers per oval-shaped gold nanoparticle.

To modify the gold nanoparticle surface by amine groups (as shown in Scheme 1), we added 30 mM cystamine dihydrochloride to 50 mL of gold nanoparticle, and the solution was kept at 50 °C for several hours under constant sonication. After that, the excess cystamine dihydrochloride was removed by centrifugation at 8000 rpm for several minutes. For covalent immobilization of the monoclonal anti- HER2/c-erb-2 antibody onto the amine, we used a highly established glutaraldehyde spacer method.[30,43] To remove the excess antibody, we the washed aptamers and anti-HER2/c-erb-2 antibody-conjugated nanoparticles several times with PBS. To measure the number of anti-HER2/c-erb-2 antibody molecules in each gold nanoparticle, we performed the above process with Rh-6G-labeled anti-HER2/c-erb-2 antibody. After conjugation, we performed exactly the same process as we did for Cy3-labeled aptamers. The amount of Rh-6G-labeled anti-HER2/c-erb-2 antibody was measured by fluorescence. By dividing the total number of Rh-6G-labeled anti-HER2/c-erb-2 antibody by the total number of nanoparticles, we estimated that there were about 70−80 anti-HER2/c-erb-2 antibodies per oval-shaped gold nanoparticle. During aptamer conjugation and immobilization of the antibody, we did not note any aggregation of gold nanoparticles as examined by TEM (as shown in Figure 8A) and UV−visible absorption spectroscopy (as shown in Figure 8B).

Cell Culture and Cellular Incubation with Multifunctional Nanoparticles. Cancer cells were grown in McCoy's 5a medium (ATCC, Rockville, MD) supplemented with 10% premium fetal bovine serum (FBS) (Lonza, Walkersville, MD) and antibiotics (10 IU/mL penicillin) in 75 cm^2 tissue culture flasks (Falcon; Becton Dickinson Labware Europe, Meylan, France) at 37 °C under 5% CO_2/95% O_2 in a humidified incubator. Before the experiments, the cells were resuspended at a concentration of 1 × 10^6 cells/mL in PBS buffer medium. An enzyme-linked immunosorbent assay kit was used to quantify HER2 in different tested cells. Our experimental results indicate that the amount of HER2 in SK-BR-3 cells was 480 ng/mL, whereas the HER2 amount was only 80 pg/mL in the case of HaCaT noncancerous cells. In the case of MDA-MB-231 cells, we found that the HER2 level was 590 pg/mL.

Different numbers of cells were then immersed into the multifunctional oval-shaped gold nanoparticle solution for 30 min at room temperature before performing the experiment.

Two-Photon Rayleigh Scattering Spectroscopy. Detailed experimental setup for the TPS experiment has been reported previously.[27,28,43,55,56] For the TPS or hyper-Rayleigh scattering (HRS) experiment, we used a mode-locked Ti:sapphire laser delivering a fundamental wavelength of 860 nm with a pulse duration of about 150 fs at a repetition rate of 80 MHz. We performed TEM data analysis before and after exposure of about 5−10 min to the laser, and we did not note any photothermal damage from multifunctional oval-shaped gold nanoparticles

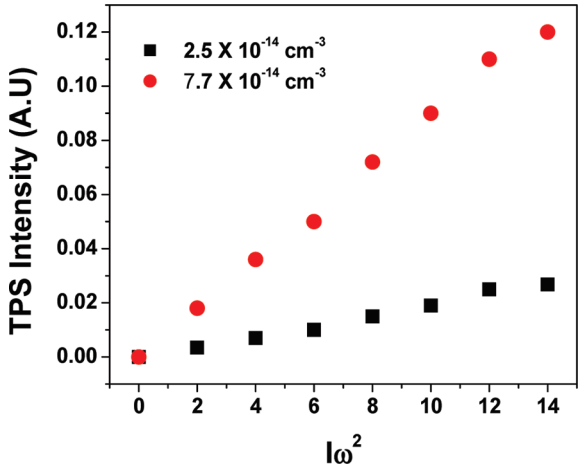

Figure 9. Power dependence of scattering intensity for different concentrations of multifunctional gold nanoparticles.

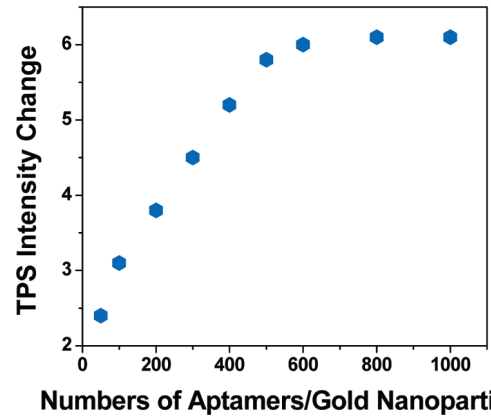

Figure 10. Aptamer concentration dependent TPS intensity change after addition of SK-BR-3 cells.

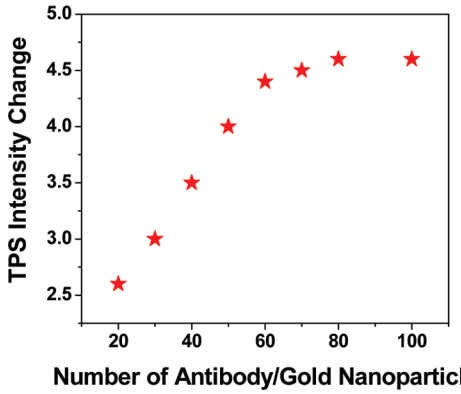

Figure 11. Anti-HER2/c-erb-2 antibody concentration dependent TPS intensity change after addition of SK-BR-3 cells.

within our TPS data collecting time. The TPS light was separated from its linear counterpart by a high-pass filter, 3 nm bandwidth interference filter, and a monochromator and then detected it with a cooled photomultiplier tube. The pulses were counted with a photon counter.

The fundamental input beam was linearly polarized, and the input angle of polarization was selected with a rotating half-wave plate. Since λ_{max} values for multifunctional oval-shaped gold nanoparticles (550 nm) and aggregates (700 nm) are very far from the excitation source (860 nm) or second harmonic generated frequency (430 nm), we can eliminate the two-photon luminescence (TPL) contributions in our HRS experiment. To make sure that only the second harmonic signal is collected by PMT, we have used a 3 nm interference filter and a monochromator in front of PMT. To understand whether the two-photon scattering intensity at 430 nm light is due to second harmonic generation, we performed power dependent as well as concentration dependent studies (as shown in Figure 9). A linear nature of the plot implies that the doubled light is indeed due to the two-photon Rayleigh scattering signal.

Aptamer Concentration Dependent Sensitivity of the TPS Probe. To understand how the sensitivity of our TPS probe varies with the concentration of the aptamer conjugated to each oval-shaped gold nanoparticle, we performed the TPS experiment with different numbers of conjugated aptamers in the presence and absence of SK-BR-3 cell lines. Figure 10 shows how the TPS intensity change varies after addition of SK-BR-3 cells when the number of aptamers/gold nanoparticles changes from 200 to 1000 aptamers/oval-shaped gold nanoparticle. Our result clearly shows that TPS intensity changes until 500−600 aptamers/gold nanoparticles and then remains unchanged. As a result, we have used 600 aptamers/oval-shaped gold nanoparticle for our experiments.

Anti-HER2/c-erb-2 Antibody Concentration Dependent Sensitivity of the TPS Probe. To understand how the sensitivity of our TPS probe varies with the concentration of the anti-HER2/c-erb-2 antibody conjugated in each oval-shaped gold nanoparticle, we also performed a TPS experiment with different numbers of conjugated anti-HER2/c-erb-2 antibodies in the presence and absence of SK-BR-3 cell lines. Figure 11 shows how the TPS intensity change varies after addition of SK-BR-3 cells when the number of anti-HER2/c-erb-2 antibody/gold nanoparticle changes from 20 to 100 antibody/oval-shaped gold nanoparticle. Our result indicates that TPS intensity changes until 70−80 anti-HER2/c-erb-2 antibody/gold nanoparticle and then remains unchanged. To get the maximum sensitivity, we have used 80 antibody/oval-shaped gold nanoparticle for our experiments.

Acknowledgment. P.C.R. thanks NIH-SCORE Grant No. S06GM 008047 and NSF-PREM Grant No. DMR-0611539 for their generous funding. We also thank reviewers whose valuable suggestions improved the quality of manuscript.

REFERENCES AND NOTES

1. Chen, H -Zi; Tsai, S-Y; Leone, G. Emerging Roles of E2FS In Cancer: An Exit From Cell Cycle Control. *Nat. Rev. Cancer* **2009**, *9*, 785–797.
2. Sarkar, B.; Dosch, J.; Simeone, D. M. Cancer Stem Cells: A New Theory Regarding a Timeless Disease. *Chem. Rev.* **2009**, *109*, 3200–3208.
3. Ljungman, M. Targeting the DNA Damage Response in Cancer. *Chem. Rev.* **2009**, *109*, 2929–2950.
4. http://www.cancer.gov/cancertopics/types/breast.
5. King, S. H.; Huh, Y. M.; Kim, S.; Lee, D.-K. Isolation of RNA Aptamers Targeting HER-2-Overexpressing Breast Cancer Cells Using Cell-SELEX. *Bull. Korean Chem. Soc.* **2009**, *30*, 1827–1831.
6. Lal, S.; Clare, S. E.; Halas, N. J. Nanoshell-Enabled Photothermal Cancer Therapy: Impending Clinical Impact. *Acc. Chem. Res.* **2008**, *41*, 1842–1851.
7. Nam, J.; Won, N.; Jin, H.; Chung, H.; Kim, S. pH-Induced Aggregation of Gold Nanoparticles for Photothermal Cancer Therapy. *J. Am. Chem. Soc.* **2009**, *131*, 13639–13645.
8. Yong, K.-T.; Ding, H.; Roy, I.; Law, W.-C.; Bergey, E. J.; Maitra, A.; Prasad, P. N. Imaging Pancreatic Cancer Using Bioconjugated InP Quantum Dots. *ACS Nano* **2009**, *3*, 502–510.
9. Bhirde, A. A.; Patel, V.; Gavard, J.; Zhang, G.; Sousa, A. A.; Masedunskas, A.; Leapman, R. D.; Weigert, R.; Gutkind, S. J.; Rusling, J. F. Targeted Killing of Cancer Cells *In Vivo* and *In Vitro* with EGF-Directed Carbon Nanotube-Based Drug Delivery. *ACS Nano* **2009**, *3*, 307–316.
10. Fang, Z.; Soleymani, L.; Pampalakis, G.; Yoshimoto, M.; Squire, J. A.; Sargent, E. H.; Kelley, S. O. Direct Profiling of Cancer Biomarkers in Tumor Tissue Using a Multiplexed Nanostructured Microelectrode Integrated Circuit. *ACS Nano* **2009**, *3*, 3207–3213.
11. Liu, X.; Dai, Q.; Austin, L.; Coutts, J.; Knowles, G.; Zou, J.; Chen, H.; Huo, Q. A One-Step Homogeneous Immunoassay for Cancer Biomarker Detection Using Gold Nanoparticle Probes Coupled with Dynamic Light Scattering: pH-Induced Aggregation of Gold Nanoparticles for Photothermal Cancer Therapy. *J. Am. Chem. Soc.* **2008**, *130*, 2780–2782.
12. Agasti, S. S.; Chompoosor, A.; Chang-Cheng, Y.; Ghosh, P.; Kim, C. K.; Rotello, V. M. Photoregulated Release of Caged Anticancer Drugs from Gold Nanoparticles. *J. Am. Chem. Soc.* **2009**, *131*, 5728–5729.
13. Stoeva, S. I.; Lee, J.-S.; Smith, J. E.; Rosen, S. T.; Mirkin, C. A. Multiplexed Detection of Protein Cancer Markers with Biobarcoded Nanoparticle Probes. *J. Am. Chem. Soc.* **2006**, *128*, 8378–8379.
14. Erogbogbo, F; Yong, K.-T.; Roy, I.; Xu, G.; Prasad, P. N.; Swihart, M. T. Biocompatible Luminescent Silicon Quantum Dots for Imaging of Cancer Cells. *ACS Nano* **2008**, *2*, 873–878.
15. Vigneshwaran, M.; Bhaskara, V. C.; Vyomesh, P.; Silvio, G. J.; James, F. R. Ultrasensitive Immunosensor for Cancer Biomarker Proteins Using Gold Nanoparticle Film Electrodes and Multienzyme-Particle Amplification. *ACS Nano* **2009**, *3*, 585–594.
16. Chen, X.; Estévez, M. C.; Zhu, Z.; Huang, Y. F.; Chen, Y.; Wang, L.; Weihong, T. Using Aptamer-Conjugated Fluorescence Resonance Energy Transfer Nanoparticles for Multiplexed Cancer Cell Monitoring. *Anal. Chem.* **2009**, *81*, 7009–7014.
17. Shamah, S. M.; Healy, J. M.; Cload, S. T. Complex Target SELEX. *Acc. Chem. Res.* **2008**, *41*, 130–138.
18. Huang, X.; El-Sayed, I.; Qian, W.; El-Sayed, M. A. Cancer Cell Imaging and Photothermal Therapy in the Near-Infrared Region by Using Gold Nanorods. *J. Am. Chem. Soc.* **2006**, *128*, 2115–2120.
19. Moon, H. K.; Lee, S. H.; Choi, H. C. *In Vivo* Near-Infrared Mediated Tumor Destruction by Photothermal Effect of Carbon Nanotubes. *ACS Nano* **2009**, *3*, 3707–3713.

20. Huang, Y.-F.; Liu, H.; Xiong, X.; Chen, Y.; Tan, W. Nanoparticle-Mediated IgE-Receptor Aggregation and Signaling in RBL Mast Cells. *J. Am. Chem. Soc.* **2009**, *131*, 17328–17334.
21. Gil, P. R.; Parak, W. J. ACS Nano, Composite Nanoparticles Take Aim at Cancer. *ACS Nano* **2008**, *2*, 2200–2205.
22. Liu, X.; Dai, Q.; Austin, L.; Coutts, J.; Knowles, G.; Zou, J.; Chen, H.; Huo, Q. A One-Step Homogeneous Immunoassay for Cancer Biomarker Detection Using Gold Nanoparticle Probes Coupled with Dynamic Light Scattering. *J. Am. Chem. Soc.* **2008**, *130*, 2780–2782.
23. Xie, C.; Xu, F.; Huang, X.; Dong, C.; Ren, J. Single Gold Nanoparticles Counter: An Ultrasensitive Detection Platform for One-Step Homogeneous Immunoassays and DNA Hybridization Assays. *J. Am. Chem. Soc.* **2009**, *131*, 12763–12770.
24. Prigodich, A. E.; Seferos, D. S.; Massich, M. D.; Giljohann, D. A.; Lane, B. C.; Mirkin, C. A. Nano-flares for mRNA Regulation and Detection. *ACS Nano* **2009**, *3*, 2147–2152.
25. Wang, H.; Yang, R.; Yang, L.; Tan, W. Nucleic Acid Conjugated Nanomaterials for Enhanced Molecular Recognition. *ACS Nano* **2009**, *3*, 2451–2460.
26. Zheng, D.; Seferos, D. S.; Giljohann, D. A.; Patel, P. C.; Mirkin, C. A. Aptamer Nano-flares for Molecular Detection in Living Cells. *Nano Lett.* **2009**, *9*, 3258–3261.
27. Ray, P. C. Label-Free Diagnostics of Single Base-Mismatch DNA Hybridization on Gold Nanoparticles Using Hyper-Rayleigh Scattering Technique. *Angew. Chem., Int. Ed* **2006**, *45*, 1151–1154.
28. Darbha, G. K.; Rai, U. S.; Singh, A. K.; Ray, P. C. Highly Selective Detection of Hg^{2+} Ion Using NLO Properties of Gold Nanomaterial. *J. Am. Chem. Soc.* **2008**, *130*, 8038–8042.
29. Nie, S.; Emory, S. R. Probing Single Molecules and Single Nanoparticles by Surface-Enhanced Raman Scattering. *Science* **1997**, *275*, 1102–1106.
30. Bell, S. E. J.; Sirimuthu, N. M. S. Surface-Enhanced Raman Spectroscopy (SERS) for Sub-micromolar Detection of DNA/RNA Mononucleotides. *J. Am. Chem. Soc.* **2006**, *128*, 15580–15581.
31. Faulds, K.; McKenzie, F.; Smith, W. E.; Graham, D. Quantitative Simultaneous Multianalyte Detection of DNA by Dual-Wavelength Surface-Enhanced Resonance Raman Scattering. *Angew. Chem., Int. Ed.* **2007**, *46*, 1829–1831.
32. Lin, Z. H.; Chang, H. T. Preparation of Gold−Tellurium Hybrid Nanomaterials for Surface-Enhanced Raman Spectroscopy. *Langmuir* **2008**, *24*, 365–367.
33. Sha, M. Y.; Xu, H.; Natan, M. J.; Cromer, R. Surface-Enhanced Raman Scattering Tags for Rapid and Homogeneous Detection of Circulating Tumor Cells in the Presence of Human Whole Blood. *J. Am. Chem. Soc.* **2008**, *130*, 17214–17215.
34. Lutz, B. R.; Dentinger, C. E.; Nguyen, L. N.; Sun, L.; Zhang, J.; Allen, A. N.; Chan, S.; Knudsen, B. S. Spectral Analysis of Multiplex Raman Probe Signatures. *ACS Nano* **2008**, *2*, 2306–2314.
35. Kim, J. H.; Kim, J. S.; Choi, H.; Lee, S. M.; Jun, B. H.; Yu, K. N.; Kuk, E.; Kim, Y. K.; Jeong, D. H.; Cho, M. H.; Lee, Y. S. Nanoparticle Probes with Surface Enhanced Raman Spectroscopic Tags for Cellular Cancer Targeting. *Anal. Chem.* **2006**, *78*, 6967–6973.
36. Chon, H.; Lee, S.; Son, S. W.; Oh, C. H.; Choo, J. Highly Sensitive Immunoassay of Lung Cancer Marker Carcinoembryonic Antigen Using Surface-Enhanced Raman Scattering of Hollow Gold Nanospheres. *Anal. Chem.* **2009**, *81*, 3029–3034.
37. Le Ru, E. C.; Blackie, E.; Meyer, M.; Etchegoin, P. G. Surface Enhanced Raman Scattering Enhancement Factors: A Comprehensive Study. *J. Phys. Chem. C* **2007**, *111*, 13794–13803.
38. Fang, Y.; Seong, N. K. ; Dlott, D. D. Measurement of the Distribution of Site Enhancements in Surface-Enhanced Raman Scattering. *Science* **2008**, *321*, 388–392.
39. Bonham, A. J.; Braun, G.; Pavel, I.; Moskovits, M.; Reich, N. O. Detection of Sequence-Specific Protein−DNA Interactions *via* Surface Enhanced Resonance Raman Scattering. *J. Am. Chem. Soc.* **2007**, *129*, 14572–14573.
40. Dieringer, J. A.; Lettan, R. A., II; Scheidt, K. A.; Van Duyne, R. P. A Frequency Domain Existence Proof of Single-Molecule Surface-Enhanced Raman Spectroscopy. *J. Am. Chem. Soc.* **2007**, *129*, 16249–16256.
41. Dasary, S. R.; Singh, A. K.; Senapati, D.; Yu, H.; Ray, P. C. Gold Nanoparticle Based Label-Free SERS Probe for Ultrasensitive and Selective Detection of Trinitrotoluene. *J. Am. Chem. Soc.* **2009**, *131*, 13806–13812.
42. Wei, W.; Li, S.; Millstone, J. E.; Banholzer, M. J.; Chen, X.; Schatz, G. C.; Mirkin, C. A. Surprisingly Long-Range Surface-Enhanced Raman Scattering (SERS) on Au−Ni Multisegmented Nanowires. *Angew. Chem., Int. Ed.* **2009**, *48*, 4210–4212.
43. Neely, A.; Perry, C.; Varisli, B.; Singh, A. K.; Arbneshi, T.; Senapati, D.; Kalluri, J. K.; Ray, P. C. Ultrasensitive and Highly Selective Detection of Alzheimer's Disease Biomarker Using Two-Photon Rayleigh Scattering Properties of Gold Nanoparticle. *ACS Nano* **2009**, *3*, 2834–2840.
44. Griffin, J.; Singh, A. K.; Senapati, D.; Rhodes, P.; Mitchell, K.; Robinson, B.; Yu, E.; Ray, P. C. Size and Distance Dependent NSET Ruler for Selective Sensing of Hepatitis C Virus RNA. *Chem.—Eur. J.* **2009**, *15*, 342–351.
45. Mallouk, T. E.; Yang, P. Chemistry at the Nano-Bio Interface. *J. Am. Chem. Soc.* **2009**, *131*, 7937–7939.
46. Ni, W.; Kou, X.; Yang, Z.; Wang, J. Tailoring Longitudinal Surface Plasmon Wavelengths, Scattering and Absorption Cross-Sections of Gold Nanorods. *ACS Nano* **2008**, *2*, 677–686.
47. Chou, I.-H.; Benford, M.; Beier, H. T. Cot; G, L. Nanofluidic Biosensing for β-Amyloid Detection Using Surface Enhanced Raman Spectroscopy. *Nano Lett.* **2008**, *8*, 1729–1735.
48. Daniel, W. L.; Han, M. S.; Lee, J. S.; Mirkin, C. A. Colorimetric Nitrite and Nitrate Detection with Gold Nanoparticle Probes and Kinetic End Points. *J. Am. Chem. Soc.* **2009**, *131*, 6362–6363.
49. Donath, E. Biosensors: Viruses for Ultrasensitive Assays. *Nat. Nanotechnol.* **2009**, *4*, 215–216.
50. Darbha, G. K.; Ray, A.; Ray, P. C. Gold-Nanoparticle-Based Miniaturized FRET Probe for Rapid and Ultra-sensitive Detection of Mercury in Soil, Water and Fish. *ACS Nano* **2007**, *3*, 208–214.
51. Griffin, J.; Singh, A. K.; Senapati, D.; Lee, E.; Gaylor, K.; Boone, J. J.; Ray, P. C. Sequence Specific HCV-RNA Quantification Using Size Dependent Nonlinear Optical Properties of Gold Nanoparticles. *Small* **2009**, *5*, 839–845.
52. Antoine, I. R.; Benichou, E.; Bachelier, G.; Jonin, C.; Brevet, P. F. Multipolar Contributions of the Second Harmonic Generation from Silver and Gold Nanoparticles. *J. Phys. Chem. C* **2007**, *111*, 9044–9048.
53. Chandra, M.; Indi, S.; Das, P. K. Depolarized Hyper-Rayleigh Scattering from Copper Nanoparticles. *J. Phys. Chem. C* **2007**, *111*, 10652–10656.
54. Dadap, J. I.; Shan, J.; Eisenthal, K. B.; Heinz, T. F. Second-Harmonic Rayleigh Scattering from a Sphere of Centrosymmetric Materials. *Phys. Rev. Lett.* **1999**, *83*, 4045.
55. Darbha, G. K.; Rai, U. S.; Singh, A. K.; Ray, P. C. Gold Nanorod Based Sensing of Sequence Specific HIV-1 Virus DNA Using Hyper Rayleigh Scattering Spectroscopy. *Chem.—Eur. J.* **2008**, *14*, 3896–3903.
56. Singh, A. K.; Senapati, D.; Wang, S.; Griffin, J.; Neely, A.; Candice, P.; Naylor, K. M.; Varisli, B.; Kalluri, J. R.; Ray, P. C. Gold Nanorod Based Selective Identification of *Escherichia coli* Bacteria Using Two-Photon Rayleigh Scattering Spectroscopy. *ACS Nano* **2009**, *3*, 1906–1912.
57. Duboisset, I. R-A.; Benichou, E.; Bachelier, G.; Jonin, C.; Brevet, P. F. Single Metallic Nanoparticle Sensitivity with Hyper Rayleigh Scattering. *J. Phys. Chem. C* **2009**, *113*, 13477–13481.

58. Reeve, J. E.; Collins, A. H.; Mey, K. D.; Kohl, M. M.; Thorley, K. T.; Paulsen, O.; Clays, K.; Anderson, H. L. Modulated Conjugation as a Means of Improving the Intrinsic Hyperpolarizability. *J. Am. Chem. Soc.* **2009**, *131*, 2758–2759.
59. Das, P. K. Chemical Applications of Hyper-Rayleigh Scattering in Solution. *J. Phys. Chem. B* **2006**, *110*, 7621–7630.
60. Duncan, V.; Song, K.; Hung, S. T.; Miloradovic, I.; Nayak, A.; Persoons, A.; Verbiest, T.; Therien, M. J.; Clays, K. Molecular Symmetry and Solution-Phase Structure Interrogated by Hyper-Rayleigh Depolarization Measurements: Elaborating Highly Hyperpolarizable D_2-Symmetric Chromophores. *Angew. Chem., Int. Ed.* **2008**, *47*, 2978–2981.
61. Clays, K.; Persoons, A. Hyper-Rayleigh Scattering in Solution. *Phys. Rev. Lett.* **1991**, *66*, 2980–2983.
62. Terhune, R. W.; Maker, P. D.; Savage, C. M. Measurements of Nonlinear Light Scattering. *Phys. Rev. Lett.* **1965**, *14*, 681.
63. Oudar, J. L. Optical Nonlinearities of Conjugated Molecules. Stilbene Derivatives and Highly Polar Aromatic Compounds. *J. Chem. Phys.* **1977**, *67*, 44–49.
64. Tiwari, V. S.; Oleg, T.; Darbha, G. K.; Hardy, W.; Singh, J. P.; Ray, P. C. Non-resonance SERS Effects of Silver Colloids with Different Shapes. *Chem. Phys. Lett.* **2007**, *446*, 77–82.